Infrared intensities and Raman-scattering activities within density-functional theory

Dirk Porezag

Technische Universität, Institut für Physik, Theoretische Physik III, D-09009 Chemnitz, Germany

Mark R. Pederson

Complex Systems Theory Branch, Naval Research Laboratory, Washington, D.C. 20375

(Received 20 February 1996; revised manuscript received 22 May 1996)

We show that the computational complexity associated with the density-functional-based determination of infrared intensities and nonresonant Raman scattering activities is the same as that required for vibrational modes. Further, we use extremely large basis sets to determine the intrinsic accuracy for calculating such phenomena within the density-functional theory. We present benchmark calculations on CH_4, H_2O, C_2H_2, C_2H_4, and C_2H_6 within both the local-density approximation (LDA) and the generalized gradient approximation (GGA). Tests of the reliability and numerical stability of the theoretical scheme are presented. We show that in order to obtain reliable results, appropriate polarization basis functions and well-converged wave functions are necessary. While most of the Raman spectra predicted by LDA agree very well with experimental data, some of the infrared intensities show substantial errors. The GGA functional overcomes most of these deficiencies, leading to an overall good agreement with experiment. [S0163-1829(96)02035-8]

I. INTRODUCTION

For the last 30 years, density-functional theory (DFT) has been applied computationally to determine a great variety of different properties for numerous systems. The most widely used approach is to calculate the exchange-correlation energy in the local-density approximation (LDA).[1] Many of the strengths and weaknesses of this approximation are well known. While the LDA has proven to yield accurate geometries,[2–4] static dipole moments,[4] and vibrational frequencies,[3–7] atomization energies are typically overestimated.[3,4,8,9] Recently, functionals which also use the density gradient to determine the exchange-correlation energy (generalized gradient approximation, GGA) have been shown to overcome the LDA deficiencies partially. A considerable amount of work has already been done to test the performance of the GGA for calculations of total energies, geometries, vibrational frequencies, and reaction barriers.[3,4,8,10–14] In addition to developing accurate density-functional-based methodologies, a parallel goal has been to develop computational schemes which scale favorably as a function of system size, and today there are many researchers actively engaged in developing algorithms for this purpose.[15–17] In this work we address the density-functional-based determination of Raman-scattering activities and infrared-absorption intensities from both of these standpoints.

While there has been much effort aimed at calculating vibrational modes within density-functional theory most of the theoretical tools used for vibrational intensities have employed semiempirical methods or the empirical bond polarization model for large molecules such as fullerenes,[18,19] or traditional quantum-chemistry methodologies such as the Hartree-Fock or Moller-Plessent perturbation theory for smaller molecules.[20–25] The majority of the quantum-chemistry-based investigations were directed toward infrared absorption, leading to theoretically determined intensities that typically deviate 10–50% from the experimental values, depending on the particular vibration and the level of theory. We also note that while the most recent version of the GAUSSIAN codes may allow for the calculation of infrared and Raman spectra within DFT, there has not yet been an effort aimed at determining the intrinsic accuracy of DFT for such phenomena. With respect to the latter goal, we note that such quantities are not variational, so it is necessary to use significantly larger basis sets and stricter convergence criteria to determine quantitatively precisely what size basis sets are required for such calculations. The Gaussian-based electronic structure codes of Pederson and co-workers[26–29] are well suited for this type of investigation, since it is easy to include basis sets of arbitrary size.

The ability to determine infrared absorption intensities and Raman scattering activities quickly and accurately from first principles will be very useful for investigating and characterizing additional materials, since vibrational spectroscopy is one of the most powerful experimental techniques that is used in contemporary materials research.

In Sec. II, we discuss the computational and theoretical details associated with the calculation of infrared and Raman spectroscopy. A primary point of this work is that, once the dynamical matrix associated with a given system is obtained, it is possible to determine the infrared and Raman spectra with a total of 12 additional calculations regardless of system size. In Sec. III, we present GGA and LDA results for five molecules, and compare with experiment. In addition to the peak heights, we also present results for polarizabilities and dipole moments. We end with some conclusions in Sec. IV.

II. COMPUTATIONAL AND THEORETICAL DETAILS

A. Infrared absorption and Raman-scattering intensities

Here we will give only a short summary of the theory our calculations are based on. For more detailed studies, we rec-

ommend Refs. 30 and 31. In the harmonic approximation, the vibrational eigenmodes of a given system can be found by solving the eigenvalue problem

$$\sum_{k=1}^{3N} (H_{jk} - \lambda_i M_{jk}) X_{ki} = 0, \quad j=1\ldots 3N, \quad \lambda_i = (2\pi\nu_i)^2,$$

$$\sum_{k=1}^{3N} \sum_{l=1}^{3N} X_{ki} M_{kl} X_{lj} = \delta_{ij}, \quad (1)$$

$$M_{kl} = \delta_{kl} m_n, \quad k = 3n-2, 3n-1, 3n.$$

In Eq. (1), N is the number of atoms, H is the dynamical or hessian matrix of the system, X_{ki} are the elements of the ith eigenvector, m_n is the mass of the nth atom and ν_i is the frequency of the ith mode. A displacement U_{ki} in the direction of the ith eigenvector can then be written as

$$U_{ki} = Q_i X_{ki}. \quad (2)$$

Q_i is referred to as a normal-mode coordinate. Often, the derivatives of some physical property A with respect to Q_i are required. If the derivatives of A are already known with respect to the external (Cartesian) atomic coordinates R_k, the required expression can easily be obtained from

$$\frac{dA}{dQ_i} = \sum_{k=1}^{3N} \frac{\partial A}{\partial R_k} X_{ki}. \quad (3)$$

Following Ref. 30, the first-order infrared intensity of the ith mode is given by

$$I_i^{\mathrm{IR}} = \frac{\mathcal{N}\pi}{3c} \left| \frac{d\boldsymbol{\mu}}{dQ_i} \right|^2 \quad (4)$$

where $\mathcal{N}$ is the particle density, c is the velocity of light and $\boldsymbol{\mu}$ is the electric dipole moment of the system. Since $|d\boldsymbol{\mu}/dQ_i|^2$ is the only molecular property entering the formula, it is often also referred to as absolute infrared intensity. For that reason, one finds different units for I^{IR} in the literature: 1 (D/Å)^{2}amu$^{-1} = 42.255$ km/mol $= 171.65$ cm^{-2} atm^{-1} at $0\,^\circ$C and 1 atm.[23]

The evaluation of Raman-scattering intensities is slightly more complicated. Following Refs. 32 and 33, the first-order differential Raman cross section for the Stokes component of the ith eigenmode far from resonance is given by

$$\frac{d\sigma_i}{d\Omega} = \frac{(2\pi\nu_S)^4}{c^4} \left| \hat{e}_S \frac{\partial\widetilde{\alpha}}{\partial Q_i} \hat{e}_L \right|^2 \frac{h(n_i^b + 1)}{8\pi^2\nu_i},$$

$$n_i^b = \left[\exp\left(\frac{h\nu_i}{kT}\right) - 1 \right]^{-1}. \quad (5)$$

In Eq. (5), ν_S is the frequency of the scattered light, $\hat{e}_S$ and $\hat{e}_L$ are the unit vectors of the electric-field direction (polarization) for the scattered and the incident light, $\widetilde{\alpha}$ is the polarizability tensor, and n_i^b the Bose-Einstein statistical factor. Since molecules in the gas phase may be oriented randomly, this expression has to be appropriately space averaged. The result of this averaging procedure depends on the relative orientations of the direction and polarization of the incident and scattered beams. In most experiments, a plane-polarized incident laser beam is used. Further, the direction of the incident beam, the polarization direction of this beam, and the direction of observation are perpendicular to each other. Under these circumstances, one yields a Raman cross section

$$\frac{d\sigma_i}{d\Omega} = \frac{(2\pi\nu_S)^4}{c^4} \frac{h(n_i^b + 1)}{8\pi^2\nu_i} \frac{I^{\mathrm{Ram}}}{45},$$

$$I^{\mathrm{Ram}} = 45\left(\frac{d\alpha}{dQ}\right)^2 + 7\left(\frac{d\beta}{dQ}\right)^2 = 45\alpha'^{\,2} + 7\beta'^{\,2}, \quad (6)$$

where

$$\alpha' = \tfrac{1}{3}(\widetilde{\alpha}'_{xx} + \widetilde{\alpha}'_{yy} + \widetilde{\alpha}'_{zz}),$$

$$\beta'^{\,2} = \tfrac{1}{2}[(\widetilde{\alpha}'_{xx} - \widetilde{\alpha}'_{yy})^2 + (\widetilde{\alpha}'_{xx} - \widetilde{\alpha}'_{zz})^2 + (\widetilde{\alpha}'_{yy} - \widetilde{\alpha}'_{zz})^2$$
$$+ 6(\widetilde{\alpha}'^{\,2}_{xy} + \widetilde{\alpha}'^{\,2}_{xz} + \widetilde{\alpha}'^{\,2}_{yz})], \quad (7)$$

and a depolarization ratio

$$\varrho_l = \frac{3\beta'^{\,2}}{45\alpha'^{\,2} + 4\beta'^{\,2}} \quad (8)$$

describing the ratio of the intensities perpendicular and parallel to the incident polarization. In the above equations, α' is the mean polarizability derivative, $\beta'^{\,2}$ is the anisotropy of the polarizability tensor derivative and I^{Ram} is the Raman-scattering activity. Primes denote derivatives with respect to the normal mode coordinate Q. Finally, we would like to stress that all formulas given in this section are derived within the double harmonic approximation, which means, that higher-order changes of the energy, dipole moment, and polarizability with respect to the normal-mode coordinate are neglected.

B. Computational scheme

To perform the calculations discussed here, we have used the all-electron, full potential Gaussian-orbital cluster code discussed in Refs. 26–29. The potential is calculated analytically on a variational integration mesh which allows for the determination of electronic structure, total energies, and Pulay-corrected Hellmann-Feynman forces with any desired numerical precision. We use the Perdew-Zunger parametrization for the Ceperley-Alder LDA functional,[34] and the Perdew-Wang PW GGA-II generalized gradient functional.[8,9]

Vibrational modes are determined by a direct diagonalization of the dynamical matrix. This matrix is constructed by finite differencing of the forces at different points near the equilibrium geometry. In particular, we perform for each atom and each coordinate x, y, and z two different displacements by the same small distance ($dx = 0.05$ a.u.) in the positive and negative directions of the current axis, and calculate the forces for the corresponding geometry. A more detailed description of this technique can be found in Ref. 35. We have tested the reliability of the results by repeating the calculation for some of the molecules with $dx = 0.02$ a.u., which does not lead to any significant changes in the frequencies or intensities of the vibrational modes.

C. Determination of dipole moment and polarizability derivatives

Based on the definition of dipole moment and polarizability, we calculate the derivatives of these properties with respect to the atomic coordinates as a direct response to an external electric field,

$$\left.\begin{aligned} \frac{\partial \mu_i}{\partial R_k} &= -\frac{\partial^2 E}{\partial G_i \partial R_k} = \frac{\partial F_k}{\partial G_i} \\ \frac{\partial \widetilde{\alpha}_{ij}}{\partial R_k} &= -\frac{\partial^3 E}{\partial G_i \partial G_j \partial R_k} = \frac{\partial^2 F_k}{\partial G_i \partial G_j} \end{aligned}\right\} \quad i,j = x,y,z. \quad (9)$$

In the above equation, F_k is the (Pulay-corrected) force acting on an atom, and G_j is one component of the external electric field. Thus, after finding the equilibrium geometry of the system, the dipole moment and the polarizability and their derivatives with respect to the atomic coordinates can be determined by a finite differencing of energies and forces with respect to the electric-field vector G according to Eq. (9).

The polarizability tensor has six independent variables. The dipole moment is a vector of three independent variables which can be determined simultaneously with the diagonal elements of the polarizability. In order to avoid first-order errors, the numerical differentiation for each component requires two additional self-consistent field (SCF) calculations. Thus a total of $2 \times 6 + 1 = 13$ calculations is necessary. A similar scheme was already used by Komornicki and McIver[21] in studies based on the Hartree-Fock method.

We want to note here that SCF calculations with a finite electric field are problematic at first sight: If the electric field is truly uniform, the electrons are likely to escape to infinity. However, since our Gaussian basis functions are localized at the atomic sites, and since we deal with isolated clusters or molecules, the electronic problem is limited to a finite region in space (a box). Consequently, the results would not change if the uniform electric field was replaced by a field with a wavelength much larger than the box size (using a slowly varying field eliminates the problems mentioned above).

As pointed out in Ref. 23, the Raman-scattering activity depends on a third-order derivative of the total energy [see Eq. (9)]. This means that extremely well-converged calculations will be required to obtain accurate intensities. Also, if the field strength used in the finite differencing scheme is too large, higher-order terms will lead to inaccuracies in the numerical derivatives. Further, since the exchange-correlation functionals are highly nonlinear, an accurate DFT scheme has to rely on numerical quadratures to calculate physical properties, and intrinsic numerical precision can also be an issue. These three effects will be the most important source of numerical errors in our scheme. To understand how these effects must be controlled, we have performed LDA calculations to determine the derivative of the H_2 molecule polarizability parallel to the bond with respect to the bond length and for different values of the electric field. In this test, we used a coarse and a more accurate fine integration mesh and a convergence criterion of 5×10^{-6} hartree for the *total* energy in one case and for the *kinetic* energy in the other case. Since convergence of the kinetic energy is *linear,* and convergence of the total energy is *quadratic* with the conver-
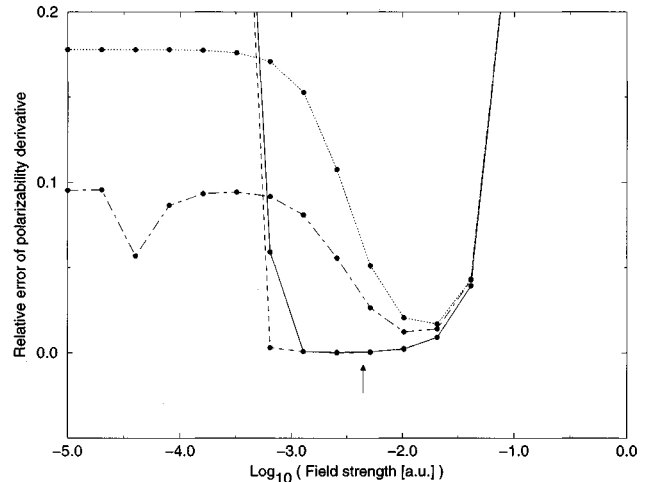

FIG. 1. Relative error of the numerically determined polarizability derivative along the H_2 molecule bond, calculated within the LDA for different values of the external electric field, different convergence criteria, and with different integration meshes. Points denote the actual calculations; the lines are intended to guide the eye. The arrow indicates a field strength of 0.005 a.u., which was used in the calculations presented here. The solid and dashed lines correspond to strict SCF convergence with coarse and fine meshes, respectively. The dotted and dashed-dotted lines correspond to weaker convergence with coarse and fine meshes, respectively. As discussed in the text, this figure shows that well-converged wave functions are extremely important in our numerical differencing scheme, while the numerical precision is less important.

gence of the wave functions, the two convergence criteria may be thought of as strict and weak, respectively. The results are displayed in Fig. 1. For field strengths larger than about 0.03 a.u., the error is determined by higher-order terms, and the three-point numerical differentiation is clearly not accurate enough. For field strengths smaller than about 0.001 a.u., the numerical integration is the main source of error. Between the upper and lower limits, the calculations with converged kinetic energies show a stable behavior. Further, coarse and fine meshes yield almost indistinguishable results. As expected, toward the lower limit, the fine mesh is slightly more accurate. However, the calculations with converged total energy do not stabilize at the right value for any field strength. This behavior has to be expected, since none of the calculated derivatives is variational in the wave functions. Therefore, it is absolutely necessary to repeat the SCF procedure until a nonvariational quantity such as the kinetic energy is converged. For the calculations discussed in Sec. III, a convergence criterion of 5×10^{-6} a.u. and a field strength of 0.005 a.u. have been used.

III. RESULTS AND DISCUSSION

Basis set dependencies of the theoretically obtained spectra have only been determined for CH_4 (see Tables I and III). For all other molecules and for the determination of the vibrational frequencies and eigenvectors, the largest basis BAS6 has been used. Further, the phonon frequencies of the test molecules are known to be well described within both the LDA and GGA. Differences between the two functionals

TABLE I. Specifications of the basis sets used in the calculation for CH_4. Basis sets BAS1–BAS5 are constructed from Gaussian exponents ranging from 0.11 to 4233 for carbon, and from 68.16 to 0.08 for hydrogen. BAS6 consists of even tempered Gaussians ranging from 0.05 to 5000 for carbon, from 10 000 to 0.05 for oxygen, and from 139 to 0.08 for hydrogen.

| | Basis functions | | | | | | Bare Gaussians | | | | | |
| | C and O | | | H | | | C and O | | | H | | |
	s	p	d	s	p	d	s	p	d	s	p	d
BAS1	2	1	0	1	0	0	10	7	0	6	0	0
BAS2	3	2	0	2	0	0	10	7	0	6	0	0
BAS3	10	7	0	6	0	0	10	7	0	6	0	0
BAS4	10	7	0	6	4	0	10	7	0	6	4	0
BAS5	10	7	4	6	4	0	10	7	4	6	4	0
BAS6	14	9	4	7	5	3	14	9	4	7	5	3

are small, usually ranging from 0 to 3 %.[4] The results presented here are either determined entirely within the LDA or entirely within the GGA. That is, the LDA results correspond to phonon eigenvectors calculated within the LDA, while the GGA results use GGA vibrational eigenvectors.

A. CH_4

To test the basis set dependency of the theoretical intensities, calculations for basis sets of different sizes have been performed within LDA for this molecule (see Table III). The basis sets are characterized in Table I. Clearly, BAS1, BAS2, and BAS3 give poor results due to the lack of polarization functions. The inclusion of p functions for the hydrogens (BAS4) significantly improves these results, leading to a static polarizability that is almost converged with respect to basis set size and close to the experimental value.[36] Also, the Raman intensities derived with BAS4 agree reasonably well

TABLE II. Static dipole moments and principal values of the optical polarizability tensor as calculated within the LDA and GGA. Experimental values are from Ref. 36, except for the polarizability of C_2H_4 that was taken from Ref. 38.

Molecule	Method	μ D	α_1	α_2 Å^3	α_3
CH_4	LDA	0	2.68	2.68	2.68
	GGA	0	2.62	2.62	2.62
	Exp	0	2.60	2.60	2.60
H_2O	LDA	1.87	1.62	1.60	1.59
	GGA	1.82	1.60	1.58	1.56
	Exp	1.84			
C_2H_2	LDA	0	4.79	2.98	2.98
	GGA	0	4.79	2.89	2.89
	Exp	0	5.12	2.43	2.43
C_2H_4	LDA	0	5.41	3.99	3.45
	GGA	0	5.39	3.91	3.44
	Exp	0	5.40	3.85	3.40
C_2H_6	LDA	0	4.98	4.35	4.35
	GGA	0	4.91	4.24	4.24
	Exp	0	5.48	3.97	3.97

with the experimental data.[37] Inclusion of d functions for the carbon atoms leads to minor changes while the inclusion of d functions for the hydrogens brings the $1T_2$ Raman activity into significantly better agreement with experiment. However, all basis sets predict the wrong ordering of the IR intensities for the two T_2 modes, indicating a systematic error of the LDA functional. This assumption is supported by a GGA calculation using the large BAS6 basis. The GGA yields much better IR intensities for both modes. Consider-

TABLE III. Vibrational frequencies, polarizabilities, infrared intensities, and Raman-scattering activities for CH_4 as calculated within the LDA and GGA using different basis sets. The basis sets are specified in Table I. Vibrational modes have only been obtained with the large BAS6 basis and the LDA. Experimental harmonic frequencies are from Ref. 4, infrared intensities from Ref. 23, and Raman scattering activities from Ref. 37.

Mode	$1T_2$	$1E$	$1A_1$	$2T_2$			
ν_{LDA} in cm^{-1}	1244	1473	2954	3082			
ν_{GGA} in cm^{-1}	1283	1509	3013	3090			
ν_{exp}^{harm} in cm^{-1}	1357	1567	3037	3158			
Basis and	$\widetilde{\alpha}$	I^{IR}		I^{Ram}			
Functional	Å^3	$(D/Å)^2$ amu^{-1}		Å^4 amu^{-1}			
		$1T_2$	$2T_2$	$1T_2$	$1E$	$1A_1$	$2T_2$
BAS1-LDA	0.878	5.141	1.714	9.06	40.3	41.3	60.6
BAS2-LDA	1.65	3.601	1.414	8.53	65.1	81.2	127
BAS3-LDA	2.12	3.689	1.356	6.61	50.1	174	196
BAS4-LDA	2.66	1.538	0.711	0.14	6.61	244	138
BAS5-LDA	2.68	1.268	0.688	0.13	5.32	242	141
BAS6-LDA	2.68	1.374	0.654	0.27	4.40	247	141
BAS6-GGA	2.62	0.928	1.322	0.24	4.88	226	142
Experiment	2.60	0.84-0.98	1.51-1.7	0.24	7.0	223	128

TABLE IV. Vibrational frequencies, infrared intensities, and Raman-scattering activities for H_2O and C_2H_2 as calculated within the LDA and GGA. Experimental harmonic frequencies are from Ref. 4, infrared intensities from Ref. 23, and Raman-scattering activities from Ref. 39.

Mode	ν cm^{-1}			I^{IR} (D/Å)^2 amu^{-1}			I^{Ram} Å^4 amu^{-1}		
	LDA	GGA	Exp	LDA	GGA	Exp	LDA	GGA	Exp
				H_2O					
$1A_1$	1534	1575	1648	1.841	1.659	1.16-1.59	0.632	0.751	
$2A_1$	3698	3694	3832	0.094	0.037	0.059	115	109	
$1B_2$	3812	3808	3943	1.742	1.212	1.00-1.42	24.8	25.9	
				C_2H_2					
$1\Pi_g$	626	603	624	0.0	0.0		4.94	4.97	
$1\Pi_u$	720	734	747	4.652	4.465	3.84-4.26	0.0	0.0	
$1\Sigma_g$	2024	2010	2011	0.0	0.0		120	115	120
$1\Sigma_u$	3323	3366	3415	2.538	2.052	1.480	0.0	0.0	
$2\Sigma_g$	3420	3464	3497	0.0	0.0		60.7	56.4	58

ing that the largest deviation between experimental and theoretical intensities is about 30 % (for the $1E$ Raman activity), the performance of the GGA can be considered very good.

B. H_2O

The static electric dipole moment calculated for water is in excellent agreement with experiment (see Table II). The LDA infrared intensities show the right ordering of the three modes. The GGA partially overcompensates for the LDA errors, but all GGA IR intensities are closer to the experimental data. Also, the large discrepancy (about 40 %) between the measured intensities as published by different groups[23] indicates that there are also significant experimental uncertainties, and that an agreement within 30–50 % can already be considered reasonably good. The GGA and LDA Raman spectra are very similar but we are unable to discuss their quality since we were unable to find reliable experimental data.

C. C_2H_2

Considering the vibrational frequencies of this molecule, there seems to be a significant disagreement for the $1\Pi_g$ mode between recent LDA studies. While Johnson, Gill, and Pople[4] reported 475 cm^{-1}, Andzelm and Wimmer[3] found 560 cm^{-1}. We calculated this value to be 626 cm^{-1}, in excellent agreement with the experimental harmonic frequency of 624 cm^{-1}. The LDA and GGA Raman activities are also in excellent agreement with experimental spectra (see Table IV). Again, the GGA leads to better IR intensities, correcting for a good part of the LDA error. Still, both IR intensities are overestimated, the $1\Pi_u$ mode by about 10 % and the $1\Sigma_u$ mode by about 30%.

D. C_2H_4

This molecule has five IR-active modes. The LDA fails to predict the right ordering between the $1B_{1u}$, $2B_{1u}$, and

TABLE V. Vibrational frequencies, infrared intensities, and Raman-scattering activities for C_2H_4 as calculated within the LDA and GGA. Experimental harmonic frequencies are from Ref. 4, infrared intensities from Ref. 23, and Raman scattering activities from Ref. 33.

Mode	ν cm^{-1}			I^{IR} (D/Å)^2 amu^{-1}			I^{Ram} Å^4 amu^{-1}		
	LDA	GGA	Exp	LDA	GGA	Exp	LDA	GGA	Exp
$1B_{2u}$	789	809	843	0.010	0.003	0.001	0.0	0.0	
$1B_{3u}$	931	944	969	2.365	2.229	1.997	0.0	0.0	
$1B_{2g}$	947	945	959	0.0	0.0		1.70	2.25	
$1A_u$	1029	1040	1044	0.0	0.0		0.0	0.0	
$1B_{3g}$	1178	1203	1245	0.0	0.0		0.013	0.035	
$1A_g$	1320	1342	1370	0.0	0.0		34.4	38.1	27
$1B_{1u}$	1389	1425	1473	0.335	0.227	0.246	0.0	0.0	
$2A_g$	1649	1638	1655	0.0	0.0		32.9	30.1	
							32.2α	29.6α	23α
$2B_{1u}$	3041	3059	3147	0.229	0.391	0.338	0.0	0.0	
$3A_g$	3054	3072	3153	0.0	0.0		254	235	
							206α	187α	175α
$2B_{3g}$	3118	3131	3232	0.0	0.0		134	130	
$2B_{2u}$	3144	3159	3234	0.228	0.461	0.615	0.0	0.0	

TABLE VI. Vibrational frequencies, infrared intensities, and Raman-scatering activities for C_2H_6 as calculated within the LDA and GGA. Experimental harmonic frequencies are from Ref. 4, infrared intensities and Raman scattering activities are from Ref. 39.

| Mode | ν | | | I^{IR} | | | I^{Ram} | | |
| | cm^{-1} | | | (D/Å)^2 amu^{-1} | | | Å^4 amu^{-1} | | |
	LDA	GGA	Exp	LDA	GGA	Exp	LDA	GGA	Exp
$1A_{1u}$	301	297	303	0.0	0.0		0.0	0.0	
$1E_u$	780	800	822	0.317	0.200	0.149	0.0	0.0	
$1A_{1g}$	1026	998	1016	0.0	0.0		9.32	10.7	13.4
$1E_g$	1151	1177	1246	0.0	0.0		0.347	0.226	0.6
$1A_{2u}$	1323	1354	1438	0.128	0.033	0.059	0.0	0.0	
$2A_{1g}$	1342	1361	1449	0.0	0.0		0.385	0.121	0.2
$2E_u$	1419	1456	1526	0.656	0.446	0.373	0.0	0.0	
$2E_g$	1420	1457	1552	0.0	0.0		17.0	16.8	17.8
$2A_{2u}$	2946	2973	3061	1.140	1.395	1.226	0.0	0.0	
$3A_{1g}$	2947	2969	3043	0.0	0.0		400	368	302
$3E_g$	3011	3022	3175	0.0	0.0		272	260	290
$3E_u$	3034	3055	3140	1.683	2.694	2.983	0.0	0.0	

$2B_{2u}$ modes. Further, the magnitude of the very weak $1B_{2u}$ IR intensity is overestimated by an order of magnitude. The GGA corrects for all these errors, resulting in a spectrum which is close to the experimental data. Although the $1B_{2u}$ IR absorption is still overestimated by a factor of 3, this has to be considered a sufficiently accurate result. Since the intensity of this mode is three orders of magnitude smaller than those of the strongest lines, small changes in the eigenvectors and polarizability derivatives with respect to external coordinates can cause a large change in the intensity of this mode (see Table V).

Experimental Raman data are only available for the A_g part of the spectrum.[33] Our calculated spectra agree well with these data with deviations ranging from 6 % to about 50 %. Again, the LDA and GGA Raman activities are similar. The only significant improvement GGA yields is the change in the $3A_g$ Raman intensity.

TABLE VII. Comparison of absolute infrared intensities [in (D/Å)^2 amu^{-1}] as calculated within the LDA and GGA (this work) and with traditional quantum-chemical methods (see Ref. 24). Note that the GGA results agree much better with the more accurate but computationally demanding CISD and CCSD(T) methods than with the Hartree-Fock (HF-SCF) scheme.

Mode	HF-SCF	CISD	CCSD(T)	LDA	GGA
		CH$_4$			
$1T_2$	0.69	0.78	0.76	1.37	0.93
$2T_2$	2.75	1.56	1.51	0.65	1.32
		H$_2$O			
$1A_1$	2.28	1.81	1.64	1.84	1.66
$2A_1$	0.39	0.19	0.11	0.09	0.04
$1B_2$	2.02	1.42	1.15	1.74	1.12
		C$_2$H$_2$			
$1\Pi_u$	5.47	4.59	4.31	4.65	4.46
$1\Sigma_u$	2.25	2.13	1.92	2.54	2.05

E. C_2H_6

The IR spectrum of C_2H_6 is already qualitatively correct described in the LDA. However, while the three weaker modes are overestimated by about 100 %, the $3E_u$ vibration is underestimated. The GGA yields better results with a maximum deviation of about 40 % for the very weak $1A_{2u}$ mode. For the stronger lines, the differences between theory and experiment ranges from 10 % to 30 % (see Table VI).

As already found for all the other molecules, the Raman spectrum is described reasonably well within the LDA with the largest error for the strong Raman lines close to 30 % (for the $3A_{1g}$ mode). The maximum deviation is reduced to about 20 % when the GGA functional is used. Larger differences occur only for the two weak $1E_g$ and $2A_{1g}$ modes. The breakdown of the $2A_{1g}$ activity is surprising when the GGA functional is applied. To make sure this is not caused by numerical problems, we have repeated the calculation with an even more accurate mesh, and found the same result. However, as was already noted earlier in this paper, anharmonic corrections will cause small changes in the vibrational eigenvectors which can lead to significant shifts in the intensities of the weak modes.

IV. CONCLUSIONS

We have tested the performance of LDA and GGA density functionals for the determination of infrared intensities and Raman-scattering activities. Four different simple hydrocarbons and a water molecule have been investigated. To the best of our knowledge, this is the first systematic attempt to derive these properties from local and gradient-corrected density functionals. While the LDA already describes the Raman spectra reasonably well, it sometimes fails to predict the right ordering of the infrared intensities. The GGA corrects for most of the LDA errors in the IR spectrum, leading to a good agreement with experimental data. In fact, as can be seen from Table VII, the GGA IR intensities also agree well with results obtained by computationally very demand-

ing quantum-chemical methods which include correlation.

Differences between the LDA and GGA Raman-scattering activities are less dramatic. As expected, modes with a large IR or Raman intensity can be described with a higher accuracy. Further, if the scheme of finite differencing with respect to an external electric field is used, reliable intensities can only be obtained with well-converged wave functions. Although basis set dependencies of the spectra have only been investigated for the CH_4 molecule, these results suggest that proper polarization functions are absolutely necessary in order to obtain a reasonable agreement with experiment. Yamaguchi *et.al.*[23] found a similar behavior in calculations of infrared intensities based on Hartree-Fock theory, and correlated methods. While it is possible that

basis set dependencies play a less important role in larger systems (for instance, Quong *et al.*[40] derived good results for the C_{60} polarizability using a *sp* basis), this remains to be seen.

[1] P. Hohenberg and W. Kohn, Phys. Rev. **136**, B864 (1964).

[2] M. R. Pederson, K. A. Jackson, and W. E. Pickett, Phys. Rev. B **44**, 3891 (1991).

[3] J. Andzelm and E. Wimmer, J. Chem. Phys. **96**, 1280 (1992).

[4] B. G. Johnson, P. M. W. Gill, and J. A. Pople, J. Chem. Phys. **98**, 5612 (1993).

[5] N. C. Handy, P. E. Maslen, R. D. Amos, J. S. Andrews, C. W. Murray, and G. J. Laming, Chem. Phys. Lett. **197**, 506 (1992).

[6] A. A. Quong, M. R. Pederson, and J. L. Feldman, Solid State Commun. **87**, 535 (1993).

[7] X. Q. Wang, C. Z. Wang, and K. M. Ho, Phys. Rev. B **48**, 1884 (1993).

[8] J. P. Perdew, J. A. Chevary, S. H. Vosko, K. A. Jackson, M. R. Pederson, D. J. Singh, and C. Fiolhais, Phys. Rev. B **46**, 6671 (1992) and references therein.

[9] J. P. Perdew and Y. Wang, Phys. Rev. B **45**, 13 244 (1992), and references therein.

[10] A. D. Becke, Phys. Rev. A **38**, 3098 (1988).

[11] B. G. Johnson, C. A. Gonzales, P. M. W. Gill, and J. A. Pople, Chem. Phys. Lett. **221**, 100 (1994).

[12] M. R. Pederson, Chem. Phys. Lett. **230**, 54 (1994).

[13] D. Porezag and M. R. Pederson, J. Chem. Phys. **102**, 9345 (1995).

[14] L. Deng, T. Ziegler, and L. Fan, J. Chem. Phys **99**, 3823 (1993).

[15] P. Ordejon, D. A. Drabold, R. M. Martin, and and M. P. Grumbach, Phys. Rev. B **48**, 14 646 (1993); **51**, 1456 (1995).

[16] F. Mauri and G. Galli, Phys. Rev. B **50**, 4316 (1994).

[17] X.-P. Li, R. W. Nunes, and D. Vanderbilt, Phys. Rev. B **47**, 10 891 (1993).

[18] D. W. Snoke and M. Cardona, Solid State Commun. **87**, 12 (1993).

[19] D. Porezag, M. R. Pederson, Th. Frauenheim, and Th. Köler, Phys. Rev. B **52**, 14 963 (1995).

[20] Recent work where quantum-chemical methods have been used to aid in the determination of structures of small silicon clusters is discussed by E. C. Honea, A. Ogura, C. A. Murray, K. Raghavachari, W. O. Sprenger, M. F. Jarrold, and W. L. Brown, Nature **366**, 42 (1993).

[21] A. Komornicki and J. W. McIver, J. Chem. Phys. **70**, 2014 (1979).

[22] M. J. Frisch, Y. Yamaguchi, J. F. Gaw, H. F. Schaefer, and J. S. Binkley, J. Chem. Phys. **84**, 531 (1986).

[23] Y. Yamaguchi, M. Frisch, J. Gaw, H. F. Schaefer, and J. S. Binkley, J. Chem. Phys. **84**, 2262 (1986), and references therein.

[24] J. R. Thomas, B. J. DeLeeuw, G. Vacek, T. D. Crawford, Y. Yamaguchi, and H. F. Schaefer, J. Chem. Phys. **99**, 403 (1993).

[25] G. E. Scuseria, J. Chem. Phys. **94**, 442 (1991).

[26] M. R. Pederson and K. A. Jackson, Phys. Rev. B **41**, 7453 (1990).

[27] M. R. Pederson and K. A. Jackson, in *Density Functional Methods in Chemistry*, edited by J. K. Labanowski and J. W. Andzelm (Springer-Verlag, Berlin, 1991).

[28] K. A. Jackson and M. R. Pederson, Phys. Rev. B **42**, 3276 (1990).

[29] M. R. Pederson and K. A. Jackson Phys. Rev. B **43**, 7312 (1991).

[30] E. B. Wilson, J. C. Decius, and P. C. Cross, *Molecular Vibrations* (McGraw-Hill, New York, 1955).

[31] D. Steele, *Theory of Vibrational Spectroscopy* (Saunders, Philadelphia, 1971).

[32] M. Cardona, in *Light Scattering in Solids*, edited by M. Cardona and G. Güntherodt (Springer-Verlag, Berlin, 1982), Vol. 50.

[33] W. F. Murphy, W. Holzer, and H. J. Bernstein, Appl. Spectrosc. **23**, 211 (1969).

[34] J. P. Perdew and A. Zunger, Phys. Rev. B **23**, 5048 (1981).

[35] M. R. Pederson, A. A. Quong, J. Q. Broughton and J. L. Feldman, Comput. Mater. Sci. **2**, 536 (1994).

[36] *Landolt-Börnstein, Numerical Data and Functional Relationships in Science and Technology*, edited by Arnold Eucken and K. H. Hellwege (Springer-Verlag, Berlin, 1951), Vol. I, Pt. 3.

[37] D. Bermejo, E. Escribano, and J. M. Orza, J. Mol. Spectrosc. **65**, 345 (1977).

[38] N. J. Bridge and A. D. Buckingham, Proc. R. Soc. London Ser. A **295**, 334 (1966); G. W. Hills and W. J. Jones, J. Chem. Soc. Faraday Trans. II **71**, 812 (1975).

[39] M. Gussoni in *Advances in Infrared and Raman Spectroscopy*, edited by R. J. H. Clark and R. E. Hester (Heyden, London, 1980), Vol. 6.

[40] A. A. Quong and M. R. Pederson, Phys. Rev. B **46**, 12 906 (1992).